Journal of Architectural Sciences and Applications
JASA 2024, 9 (1), 620-633
Research article
e-ISSN: 2548-0170
https://dergipark.org.tr/en/pub/mbud

Atmospheric and Radiometric Normalization of Satellite Images for Landscape-Level Environmental Monitoring: The Case of The Mediterranean Region

Mehmet Ali DERSE [1]*, Hakan ALPHAN [2]

ORCID 1: 0000-0001-9894-7945, **ORCID 2:** 0000-0003-1139-4087
[1, 2] *Cukurova University, Faculty of Architecture, Department of Landscape Architecture, 01330, Adana, Türkiye.*
**** e-mail**: maderse@cu.edu.tr*

Abstract

Ensuring atmospheric and radiometric consistency among the frameworks of satellite data used in regional studies is a critical requirement for change detection studies employed in regional planning monitoring. The purpose of this article is to provide a guide for the necessary atmospheric correction and radiometric normalization processes required in generating environmental data at the landscape level for physical planning. In this context, adjustments were made to remove atmospheric effects before merging multiple ASTER satellite image frames used in a project supported by TÜBİTAK, covering landscape-level environmental inventory and monitoring. The Dark Object Subtraction method with the Cos(t) model was utilized in the atmospheric correction process. Subsequently, separate regression relationships were computed for each band by considering overlapping areas on adjacent tracks of ASTER data, and radiometric normalization was performed based on these regression equations. Thus, differences between satellite images used in monitoring land changes and affecting multiple frames were minimized.

Keywords: *Radiometric normalization, land cover mapping, change detection, ASTER.*

Peyzaj Düzeyinde Çevresel İzleme İçin Uydu Verilerindeki Atmosferik ve Radyometrik Etkilerin Normalleştirilmesi: Akdeniz Bölgesi Örneği

Öz

Günümüzde onlarca faklı platform ve aygıttan çok bantlı ve yüksek yersel çözünürlüğe sahip uydu verileri sağlanmaktadır. Bölgesel çalışmalarda kullanılan uydu verilerinin çerçeveleri arasında atmosferik ve radyometrik uyumun sağlanması, bölgesel planlama çalışmalarının izlemede kullanılan değişim çalışmaları için önemli bir gereksinimdir. Bu makalenin amacı, fiziksel planlamaya peyzaj düzeyinde çevresel veri üretilmesi sürecinde gerekli olan atmosferik düzeltme ve radyometrik normalizasyon çalışması için bir rehber sunulmasıdır. Bu kapsamda TÜBİTAK tarafından desteklenen, peyzaj düzeyinde çevresel envanter ve izlemeyi kapsayan projede kullanılan birden fazla ASTER uydu görüntü çerçevesinin birleştirilmesi öncesinde, atmosferik etkilerin ortadan kaldırılması için düzeltmeler yapılmıştır. Atmosferik düzeltme işleminde Cos(t) modeli ile Koyu Obje Çıkarma (DOS) yöntemi kullanılmıştır. Daha sonra ASTER verilerinin komşu izleri üzerindeki çakışan bölgeler dikkate alınarak her bant için ayrı ayrı regresyon ilişkileri hesaplanmış, söz konusu regresyon eşitlikleri dikkate alınarak radyometrik normalizasyon yapılmıştır. Böylece arazi değişimlerinin izlemede kullanılan ve birçok çerçeveyi ilgilendiren uydu görüntüleri arasındaki farklılıklar minimuma indirilmiştir.

Anahtar kelimeler: *Radyometrik normalizasyon, arazi değişim haritalama, değişim tespiti, ASTER.*

Citation: Derse, M. A. & Alphan, H. (2024). Atmospheric and radiometric normalization of satellite images for landscape-level environmental monitoring: The case of the Mediterranean Region. *Journal of Architectural Sciences and Applications*, 9 (1), 620-633.

DOI: https://doi.org/10.30785/mbud.1446007

Received: *March 1, 2024*– ***Accepted:*** *June 25, 2024*

1. Introduction

Studies related to landscape planning and management require consistent, georeferenced, regularly obtained data covering large areas. Nowadays, information technologies comprising remote sensing and geographic information systems (GIS) offer opportunities to enhance the processes of collecting, organizing, correlating, and analyzing data pertaining to rural (Purwanto et al., 2023; Ruiz et al., 2022; Lelong & Herimandimby, 2022; Garcia-Pardo et al., 2022; El Mortaji et al., 2022; Asam et al., 2022; Gasparovic & Dobrinic, 2021; Akın & Gül, 2020; Tassri et al., 2019; Khorrami et al., 2019) and urban (Ul & Mak, 2021; Ghaseminik et al., 2021; Luo et al., 2020; Chetia et al., 2020; Tavares et al., 2019) landscapes, thus presenting significant potential for landscape planning and management processes. Consequently, these technologies facilitate the generation of numerical predictions concerning habitat conditions and changes in natural and cultural ecosystems at the level of landscape units. This enables more effective monitoring and analysis of landscape dynamics, supporting informed decision-making in various fields such as environmental management, urban planning, agriculture, forestry, and biodiversity conservation. Thus, the integration of remote sensing and GIS technologies holds promise for advancing landscape research and management practices.

Changes occurring in land cover, coastal lines, or wetland systems are among the key indicators of landscape-level changes (Rostami & Fathizad, 2022; Getachew & Manjunatha, 2022; Islam et al., 2019)

Identifying landscape-level environmental indicators and assessing them with auxiliary data layers are crucial aspects of landscape monitoring. In this context, satellite remote sensing, which has undergone significant evolution over the past approximately 50 years since its inception for civilian purposes, provides advantages such as low data and labor costs per unit area, as well as speed, repeatability, and high monitoring frequency. Presently, studies utilizing remotely sensed data are conducted in various application areas, ranging from determining temporal and spatial variability of vegetation cover (İşler & Aslan, 2021) to detecting forest fires (Karaca & Güllü, 2019). These applications demonstrate the versatility and effectiveness of remote sensing in monitoring and managing landscapes, contributing to informed decision-making and sustainable resource management practices.

Geospatially referenced resource inventories (e.g., land cover and land use maps) covering large areas and landscape-level environmental monitoring enabling change detection provide significant contributions to decision-making in planning from global to local scales (Rauf et al., 2022; Aghababaei et al., 2022; Bujan et al., 2021; Boussadia-Omari et al., 2021; Khatami et al., 2020). As evident from this description of landscape-level environmental monitoring, satellite imagery is primarily used in studies ranging from mapping land cover, detecting changes, or both, conducted at various scales from global to local. These applications underscore the importance of remotely sensed data in informing decision-making processes related to environmental management, land use planning, and sustainable development initiatives. By leveraging satellite imagery and advanced geospatial technologies, stakeholders can better understand landscape dynamics, assess environmental changes over time, and formulate evidence-based policies and strategies for effective resource management and conservation efforts.

The diversity and abundance of current satellite data does not diminish the importance of past datasets. Past data can be of critical importance as the need for information on past land cover increases in monitoring programs. In regional studies, an area of interest is generally covered by multiple scenes. Therefore, radiometric consistency between image scenes must be ensured for mapping and change detection. Inconsistencies may exist between paths and/or rows. They may also be due to different environmental conditions or sensor calibration between imaging data. Normalization of these inconsistencies is a prerequisite for many mapping and change detection studies. The objective of this paper is to provide a guide to radiometric normalization, which is essential in the production of landscape-level environmental data for spatial planning.

2. Material and Method

2.1. Material

2.1.1. Study area

The research area covers the districts of Mersin province, namely Mersin Center, Tarsus, and Erdemli, located on the Mediterranean coast of Turkey. Considering the sizes of Mersin Center, Tarsus, and Erdemli districts, the research area has a total area of 5874 km². The southern boundary of the research area is formed by the Mediterranean Sea, while the area is separated from the interior of Anatolia by the Taurus Mountains to the north. The annual average temperature of the research area is 18.7°C, while the average temperature during the winter months ranges from 9 to 15°C. The annual total precipitation amount in the area is approximately 594 mm. Characterized by a typical summer drought, December is the rainiest month, whereas August is the driest. Rainfall values measured on the coast are lower than those in the higher elevations (MGM, 2022).

The Taurus Mountains, surrounding the research area from the north, extend in an east-west direction as a high ridge between the Konya Plain of Central Anatolia and the Mediterranean. This mountain range gradually recedes from the sea towards the east of the research area, creating extensive plains between the mountains and the sea. The central districts of Mersin and Tarsus are situated in these plains. The section of the Central Taurus Mountains within the borders of Mersin province is referred to as the Bolkar Mountains. The Bolkar Mountains, with the highest peak being Mount Medetsiz (3524 m), separate the Mersin territory from the Anatolian plateau. The main characteristic of the Western and Central Taurus Mountains is their formation of high and continuous ridges, interspersed with vast plateau plains.

One of the significant geomorphological units within the research area is valleys. Rivers are deeply entrenched within these valleys. The Mediterranean climate characteristics extend from south to north along these valleys deep into the Taurus Mountains. Terraces, harboring fertile agricultural soils, are found on the slopes of these valleys. Among these valleys and plains, notable ones include the Tarsus Valley and the Tarsus and Berdan Plains.

2.1.2. Terra ASTER data

The satellite data set used in the research is derived from the Advanced Spaceborne Thermal Emission and Reflection Radiometer (ASTER) obtained through the American-Japanese joint venture TERRA satellite. In order to conduct land cover mapping for the current state of the area, seven ASTER Level 3A frames covering the entire area were utilized (Abrams et al., 2008). The ASTER data consists of 9 bands obtained at visible and near-infrared energy levels and 5 bands obtained at thermal infrared. While the visible and near-infrared bands have a spatial resolution of 15 meters, the mid-infrared data has a spatial resolution of 30 meters, and the thermal infrared data has a spatial resolution of 90 meters (Table 1) (Abrams et al., 2008).

Table 1. Band values in ASTER datasets (Abrams et al., 2008)

Band	Wavelength(μm)	Resolution (m)	Definition
VNIR_Band1	0.520 - 0.60	15	Visible-green band
VNIR_Band2	0.630 - 0.690	15	Visible-red band
VNIR_Band3N	0.760–0.860	15	near infrared band
VNIR_Band3B	0.760–0.860	15	near infrared band
SWIR_Band4	1.600–1.700	30	shortwave infrared band
SWIR_Band5	2.145–2.185	30	shortwave infrared band
SWIR_Band6	2.185–2.225	30	shortwave infrared band
SWIR_Band7	2.235–2.285	30	shortwave infrared band
SWIR_Band8	2.295–2.365	30	shortwave infrared band

Continued from Table1			
SWIR_Band9	2.360–2.430	30	shortwave infrared band
TIR_Band10	8.125–8.475	90	Longwave/thermal infrared band
TIR_Band11	8.475–8.825	90	Longwave/thermal infrared band
TIR_Band12	8.925–9.275	90	Longwave/thermal infrared band
TIR_Band13	10.250–10.950	90	Longwave/thermal infrared band
TIR_Band14	10.950–11.650	90	Longwave/thermal infrared band

ASTER data has been preferred due to its high spatial and spectral resolution. The general statistics of the data sets are provided in Table 2.

Table 2. Statistics of visible and near infrared data bands of ASTER datasets used

Data set	Date	Band	Min	Max	Ort (μ)	SD* (σ)
AST3A1_060529_0525vnir	29.05.2006	1	0	255	77,909	61,394
		2	0	255	57,159	49,909
		3N	0	255	62,984	52,828
		3B	0	255	57,359	49,048
AST3A1_060529_0526vnir	29.05.2006	1	0	255	47,383	37,329
		2	0	255	25,123	24,676
		3N	0	255	18,215	26,444
		3B	0	226	15,635	23,631
AST3A1_051109_0527vnir	09.11.2005	1	0	255	36,495	29,786
		2	0	255	20,887	21,997
		3N	0	255	15,398	19,442
		3B	0	255	17,976	23,012
AST3A1_050517_0574vnir	17.05.2005	1	0	255	96,902	74,610
		2	0	255	81,815	66,594
		3N	0	255	72,205	53,551
		3B	0	255	70,388	52,263
AST3A1_050517_0575vnir	17.05.2005	1	0	255	83,466	64,860
		2	0	255	65,682	55,848
		3N	0	255	67,287	52,155
		3B	0	228	63,668	50,510
AST3A1_060529_0576vnir	29.05.2006	1	0	255	87,838	68,422
		2	0	255	69,905	58,275
		3N	0	255	68,740	50,724
		3B	0	255	63,754	47,331
AST3A1_060824_0577vnir	24.08.2006	1	0	255	73,935	54,831
		2	0	255	55,217	44,100
		3N	0	255	52,753	39,023
		3B	0	255	54,534	40,259

*SD: Standard Deviation

2.2. Method

Regional land cover and land use mapping are increasingly being conducted with data of higher spatial resolution. However, the increase in spatial resolution leads to an increase in the amount of input data used and consequently in the number of frames used, as well as in the amount of work and time required for data processing. One of the significant stages in studies containing multiple image frames is the production of normalized image mosaics. This approach, which involves classifying a single

merged image instead of individually classifying image frames, may lead to the generation of land cover information with higher accuracy.

Image preprocessing is applied to minimize potential errors that may arise from spatial and radiometric discrepancies in satellite data before the stages of image preprocessing, classification, and change detection. In regional mapping and change detection applications where numerous datasets are processed, georegistration and radiometric correction are two critical stages of preprocessing. Georegistration involves resampling satellite data from image to image and/or entering point coordinates from the field-collected reference data and other images. Thus, the spatial coordinates in satellite data can be expressed in any projection system such as geographic latitude/longitude or Universal Transverse Mercator (UTM).

The ground coordinates collected for the georeferencing of the images were determined by considering easily identifiable features such as intersections of main roads, port/jetty facilities, and surrounding human-made objects that contrast with the environment. This information was gathered with the assistance of GARMIN GPSmap 276C. The data collected in the field with GPS were georeferenced by combining them, if necessary, with data from topographic maps.Change detection studies conducted using the radiometric properties of images generally require the use of radiometrically normalized/corrected images.

Considering the challenges of correction, relative radiometric correction is used as an alternative (Tan et al., 2012; Biday & Bhosle, 2012; Sadeghi et al., 2017)

In this approach, unlike absolute methods, simultaneous in situ measurements during satellite passage are not required. The fundamental approach in relative correction methods involves using a reference image. The radiometric properties of other images are adjusted to fit the reference dataset (Liu et al., 2022; El Hajj et al., 2008).

The Dark Object Subtraction (DOS) method is a widely used atmospheric correction technique. In this method, it is assumed that any brightness value recorded by the sensor for a pixel corresponding to a dark object or feature on the Earth's surface is due to atmospheric path radiance. The Cos(t) model incorporating the cosine of solar zenith angle (Chavez, 1996; Chavez, 1988), and an extended DOS method estimating the effects of absorption by atmospheric gases and Rayleigh scattering, are commonly employed in atmospheric correction (Chavez, 1996).

The utilization of Pseudo-Invariant Features (PIF) or Dark and Bright Pixel Clusters (DB) are among other normalization methods (Schroeder et al., 2006).

The reflection of PIFs in multiple images can be employed without the need for absolute correction of surface reflectance, ensuring that these images appear to have been acquired under the same sensor, calibration, and atmospheric conditions (Kiage et al., 2007; Liu et al., 2012).

PIF-based normalization, which involves calculating image-based linear regressions to compare images, requires the selection of target features whose reflectance values are assumed to remain constant over time. PIFs can be selected manually or automatically (Sadeghi et al., 2017; Barazzetti et al., 2016). Targets such as asphalt/concrete roads, roofs, parking lots, airports, deep lakes, dense and closed pine forests, beaches, concrete surfaces, and both new and old asphalt surfaces can be used as PIFs (Rahman et al., 2015; Yuan & Elvidge 1996; Yang & Lo, 2000).

Image-based normalization processes typically rely on linear regression models. The accuracy of georegistration is crucial when using all pixels in both images to calculate normalization coefficients. As mentioned above, customizing the comparison reflectance dataset through PIFs or "dark and bright pixel clusters" can contribute to producing more accurate results (Schott et al., 1988).

In cases where multiple images obtained at different dates are used to create a mosaic, a dataset of unchanged objects can be selected from the overlapping areas. In this study, among the 7 images from 3 adjacent paths, the images from the first path were acquired on May 17 2005, the images from the second path on May 29 2005 and the images from the third path on August 24 2006 and November 9 2005. Accordingly, the second path was considered as the reference; the images from the first and

third paths were normalized accordingly. Regression used for radiometric normalization was applied between the visible and near-infrared wavelengths of the 1st, 2nd, and 3rd bands of the ASTER data on the neighboring paths, resulting in corrected images ready for classification.

3. Research Findings and Discussion

3.1. Atmospheric Correction and Normalization Design

Since the launch of the first Landsat satellite in 1972, numerous normalization methods have been developed. A significant portion of these methods involves using a reference frame within a dataset containing multiple frames that are minimally affected by atmospheric conditions and normalizing other frames to this reference frame. These radiometric matching methods mentioned are divided into two main categories. The first category relies on generating a function that relates radiance values of the same features in the overlapping areas of two adjacent frames, while the second category is based on matching targets with a specific surface reflectance regardless of their locations.

In the first category, methods utilize different regression forms to correlate unchanged objects in overlapping areas, while in the second category, there is no requirement for the unchanged targets to be the same objects within two different frames. Regression applied to overlapping areas for the radiometric normalization of frames to be used in mosaic formation has been widely used in regional projects.

Atmospheric correction and radiometric normalization are preprocessing methods commonly required in monitoring studies with multispectral and multi-temporal coverage. These processes constitute a significant stage in monitoring studies of various geographical scopes and scales, ranging from urban change detection and monitoring (Jenerowicz et al., 2019) to detecting changes in tropical rainforests (Lobo et al., 2015), monitoring bioproductivity in grassland areas (Prieto-Amparan et al., 2018) and predicting biomass and succession in forest ecosystems (Janzen et al., 2006; Schroeder et al., 2006; Lopez-Serrano et al., 2016). Additionally, these processes are often necessary for change detection requiring time-series analyses (Gu et al., 2011).

In the study, atmospheric correction was initially performed by combining data acquired from the same paths and on the same dates for radiometric normalization of ASTER data. Subsequently, regression functions between adjacent paths were calculated, taking into account these steps, and using these regression functions, mosaics were obtained from the corrected images in the final stage (Figure 1).

The atmospheric correction process utilized a image-based method known as the Cos(t) method. This approach relies on normalizing atmospheric transmittance by accounting for the effects caused by varying solar zenith angles seasonally. Based on the calculation of the cosine of solar zenith angle, this method incorporates the advantages of the Dark Object Subtraction (DOS) method. The DOS method assumes that observed reflectance values differing from zero in satellite data for areas known to have reflectance values close to zero are due to atmospheric effects. For atmospheric correction, ASTER reflectance values were first converted to radiance values. This conversion is performed as described in Equation 1 (Pudale & Bhosle, 2007).

$$\text{Radyans} = (\text{Reflectance value} - 1) \times \text{Unit Conversion Coefficient} \quad (1)$$

The transformation coefficients for ASTER data are provided in Table 3, while the maximum radiance values are given in Table 4.

The highest and lowest reflectance values calculated for ASTER data frames, taking into account the values mentioned above, are presented in Table 5 along with the reflection values (DN pus) observed in the satellite data in areas where a zero value is expected. These values are compiled from the header files of ASTER data, which contain information such as solar elevation, date and time of data acquisition, and viewing angle.

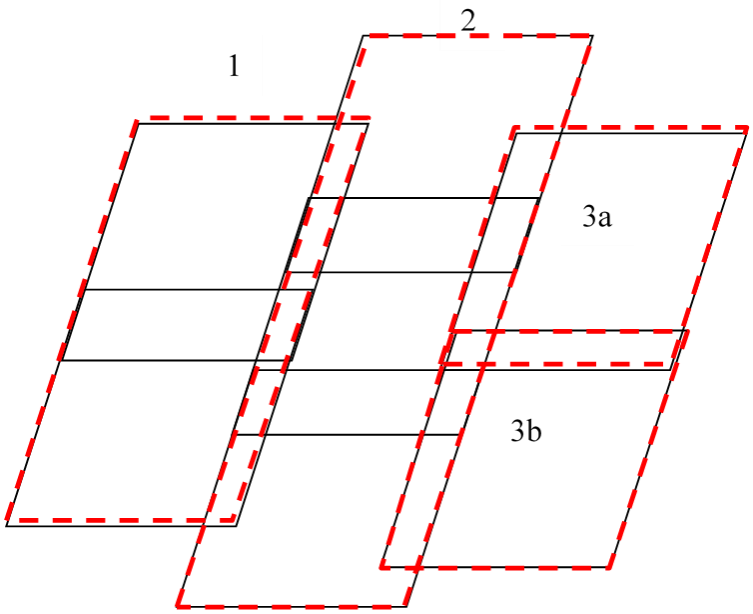

Figure 1. Reference (2) and neighboring (1, 3a, 3b) frames in radiometric normalization of aster data

Table 3. Transformation coefficients for each band in ASTER data (Pudale & Bhosle, 2007)

	Conversion Coefficient (W/(m²*sr*µm)/DN)			
Band	High gain	Normal gain	Low gain 1	Low gain 2
1	0,676	1,688	2,25	N/A
2	0,708	1,415	1,89	
3N	0,423	0,862	1,15	
3B	0,423	0,862	1,15	

Table 4. Highest radiance values for different gain values of the ASTER data bands

	Highest reflectance value (W/(m²*sr*µm)			
Band	High gain	Normal gain	Low gain 1	Low gain 2
1	170,8	427	569	N/A
2	179,0	358	477	
3N	106,8	218	290	
3B	106,8	218	290	

Table 5. Parameters used in atmospheric correction of ASTER data

Band	**Min. reflectance**	**Max. reflectance**	**DN**	**Solar**	**Time**	**Date**	**Angel**
1_1	-0,676	171,7	53	67,801853	08:36:55	17.05.2005	2,837
1_2	-0,708	179,8	22	67,801853	08:36:54	17.05.2005	2,829
1_3	-0,862	218,95	11	67,801853	08:36:54	17.05.2005	2,863
2_1	-0,676	171,7	56	69,388783	08:31:38	29.05.2006	-5,677
2_2	-0,708	179,8	24	69,388783	08:31:37	29.05.2006	-5,669
2_3	-0,862	218,95	11	69,388783	08:31:36	29.05.2006	-5,7
3a_1	-0,676	171,7	78	60,525251	08:37:16	24.08.2006	8,588
3a_2	-0,708	179,8	37	60,525251	08:37:15	24.08.2006	8,503
3a_3	-0,862	218,95	24	60,525251	08:37:14	24.08.2006	8,567
3b_1	-0,676	171,7	37	35,475225	08:34:58	09.11.2005	8,588
3b_2	-0,708	175,58	16	35,475225	08:34:57	09.11.2005	8,487
3b_3	-0,862	140,15	8	35,475225	08:34:57	09.11.2005	8,567

3.2. Testing phase

The appearance of the test area, where two different paths were merged with mosaic operations before and after this stage, is illustrated in Figure 2.

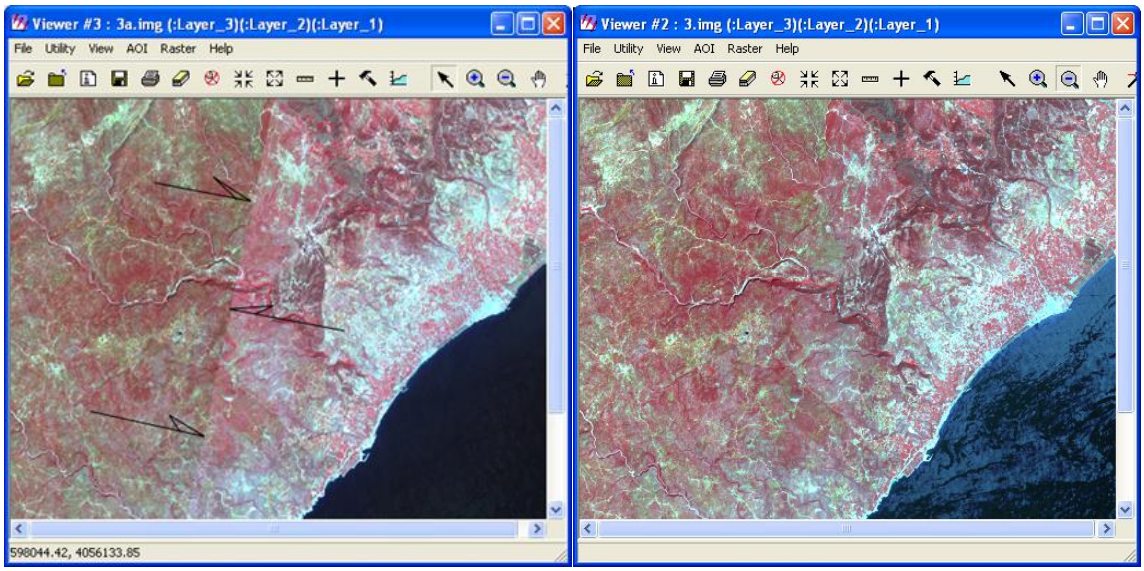

Figure 2. Mosaic images of the test area before and after normalization (the difference between neighboring traces before normalization is clearly visible)

3.3. Calculation and Merging of Corrected İmages

The regression functions used for radiometric normalization of neighboring paths of ASTER data are provided in Figure 3.

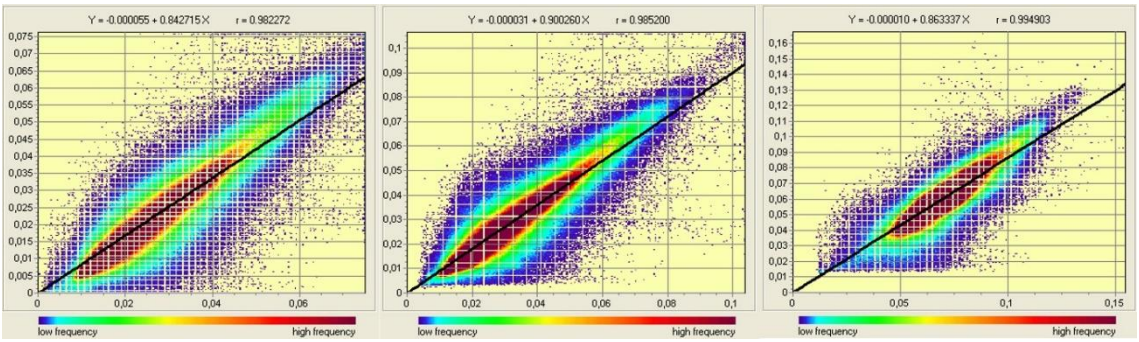

Figure 3. The regression relationship between the green (left), red (middle) and infrared (right) bands of the images in tracks 1 and 2 covering the research area

Regression functions were calculated for the neighboring frames (3a, 3b) using frame 2 as a reference, as shown in Figure 1, and after this stage, the normalized images were merged with a mosaic operation. The mosaic images before and after the regression application are presented in Figure 4.

Following radiometric normalization, the mosaic image obtained in the previous step was clipped based on the boundaries of the study area. The prepared image for classification is presented in Figure 5.

This image was obtained by displaying the 1st, 2nd, and 3rd bands (corresponding to green, red, and infrared wavelengths) as blue, green, and red (BGR), respectively, known as false color composition. In this type of visualization, areas with high reflectance due to vegetation appear with a dominant red color, highlighting vegetative features.

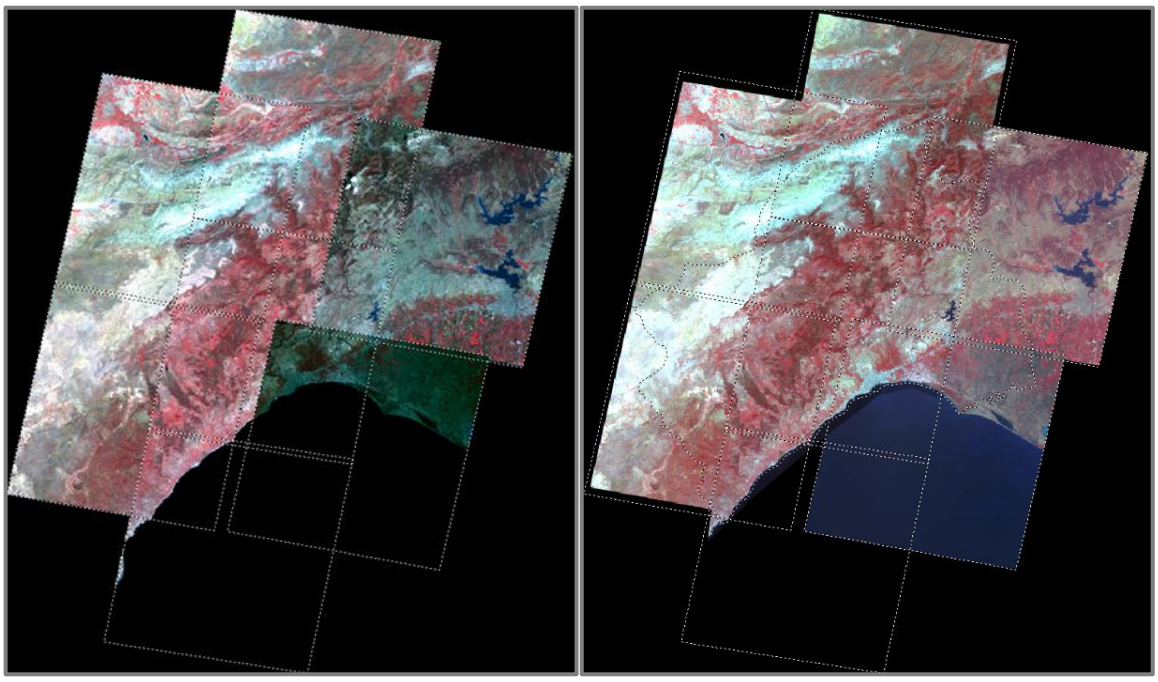

Figure 4. Mosaic images before (left) and after (right) radiometric normalization

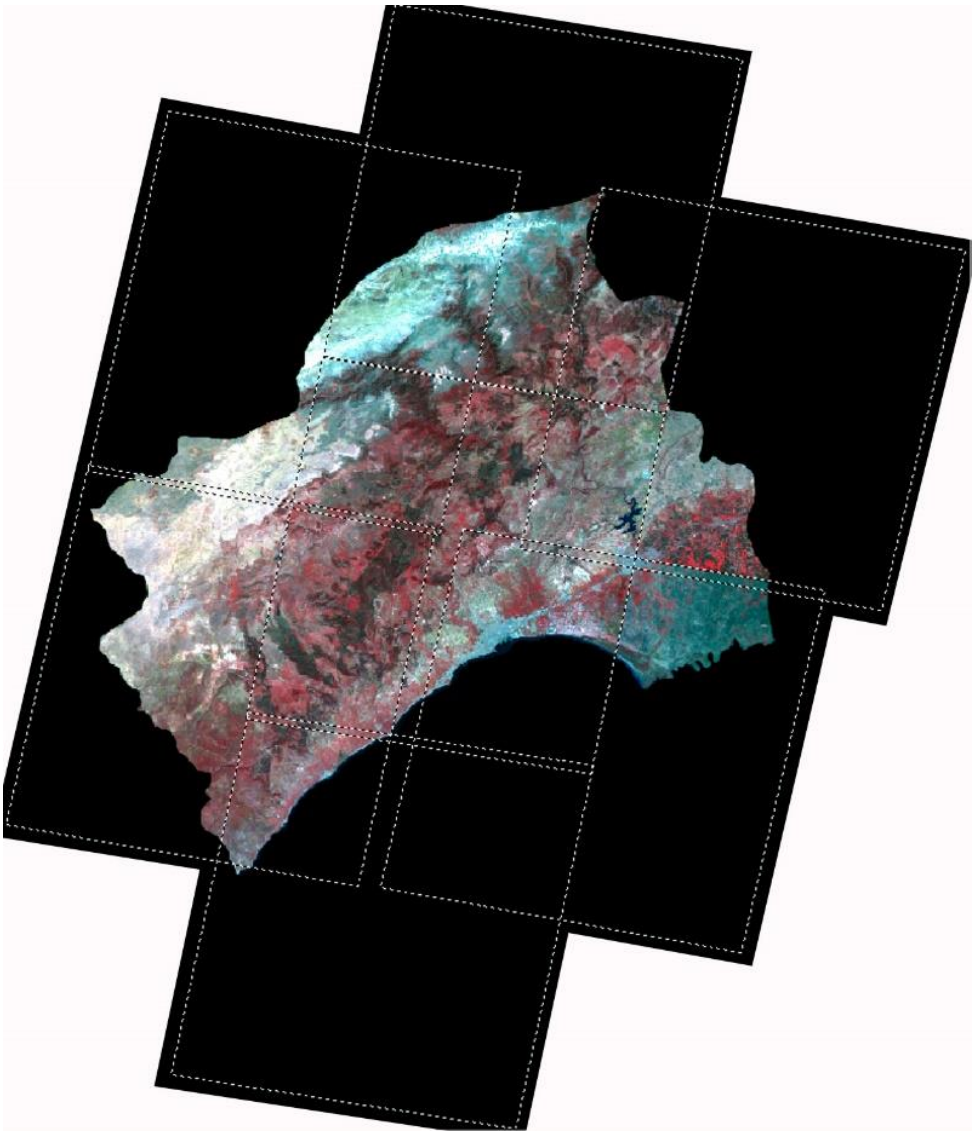

Figure 5. Radiometrically corrected aster data based on research area boundaries

In this study, seasonal effects were observed only in the southeastern part of the study area. The corresponding region comprised harvested bare agricultural fields, while the adjacent upper frame consisted of cultivated agricultural lands.
As seen in Figure 5, the reflectance values differ in the upper right and lower frames of the merged image. The image frame corresponding to the upper right corner belongs to August, while the one corresponding to the lower corner belongs to November. In the image frame from August, where agricultural fields are present, the infrared reflectance is high, hence the dominance of red color. In contrast, in the image from November covering the southern part of the same plain, where there are no crops in the agricultural fields, similar areas appear gray instead of red as observed in the upper frame.

4. Discussion and Conclusion

The potential issue with using multiple image frames in image classification lies in the high susceptibility of automatic, manual, or hybrid image classification methods applied to image mosaics created without preprocessing to errors, resulting in low thematic accuracy maps. Without correction processes applied, during the classification of merged frames, areas with similar land cover/land use (LC/LU) characteristics may be assigned different classes due to varying illumination effects and/or atmospheric conditions.

Despite the various advantages of using ASTER data in large-scale landscape mapping studies, leveraging these advantages depends on the proper preprocessing of the data frames. The primary advantage provided by the ASTER dataset, compared to LANDSAT data, is its relatively high spatial resolution and the large area coverage provided by a single image frame. The ASTER scanner, operating since the year 2000 via the EOS-Terra platform, particularly in its initial years, offered superior spatial resolution compared to other operational platform data. This superiority in spatial resolution positions ASTER data as significant for retrospective mapping and change detection studies.

Yuan & Elvidge (1996) employed Relative Radiometric Normalization (RRN), a procedure used to prepare multitemporal image datasets for detecting spectral changes associated with events such as land cover changes. This procedure reduces differences arising from unequal imaging conditions rather than changes in surface reflectance, as stated in this study. In this study utilizing Landsat data, it was noted that the linear regression technique yielded the best results (Yuan & Elvidge, 1996).

Du et al. (2002) emphasized the necessity of radiometric correction for multitemporal land cover change studies. They provided information about a new procedure for radiometric normalization in their study. They statistically selected Pseudo-Invariant Features, PIFs and utilized Principal Component Analysis, PCA for this purpose. The new procedure was applied to Landsat-5 TM images from three different years. They noted a reduction in errors in radiometric consistency among multitemporal images with this procedure (Du et al., 2002).

In their study, Scheidt et al. (2008) created an image mosaic of the study area using atmospherically corrected and radiometrically accurate ASTER data with Thermal Infrared, ASTER TIR bands for their analysis. They utilized a test site for the radiometric normalization technique. They selected Pseudo-Invariant Features, PIFs by using a correlation threshold between brightness values. They noted the advantages of this approach for TIR band data, including analyzing data obtained at different dates as a single continuous compositional dataset and separating brightness temperature from surface emission for quantitative surface composition analysis, thereby reducing errors in the intersection line in the emission mosaic (Scheidt et al., 2008).

This study presents a process for normalizing ASTER data frames for use in large-scale landscape mapping studies with a 60 km swath width. In the study, atmospheric correction was performed by combining data acquired from the same paths and on the similar dates for radiometric normalization of ASTER data. Subsequently, regression functions between adjacent paths were calculated, taking into account these steps, and using these regression functions, mosaics were obtained from the corrected images in the final stage.

In addition, the presence of seasonal variations between frames/strips and the phenological differences in vegetation cover within frames can complicate the generation of high-quality data suitable for processing. To address this issue, it may be preferable to select frames from the same seasons in such studies. In cases where this is not feasible, as mentioned in this study, it is advisable to classify separately the same land cover types exhibiting phenological differences due to seasonal effects (e.g., cultivated areas versus harvested agricultural lands).

Additionally One of the most crucial aspects in change detection studies is achieving the highest possible accuracy in geographic registration. This is because the accuracy of geographic registration directly affects the quality of intermediate products (e.g., binary masks) and final output products (e.g., change maps) generated during the change detection procedure. Failure in achieving accurate geographic registration diminishes the statistical accuracy of the study.

In summary, the correction processes presented in this study are crucial for various applications that utilize Land Cover/Land Use maps, such as environmental planning, conservation, urbanization, industrial development, tourism, transportation, and others.

Furthermore, when dealing with multiple frames/strips, seasonal variations and phenological differences within frames can pose challenges to data processing, emphasizing the importance of selecting frames from the same seasons or classifying land cover types separately based on phenological differences.

Acknowledgements and Information Note

This article was conducted within the scope of Project No. 107Y153 supported by the Scientific and Technological Research Council of Turkey (TÜBİTAK) under the 1001 Program. We would like to express our gratitude to TÜBİTAK for their financial support. The article complies with national and international research and publication ethics. Ethics Committee approval was not required for the study.

Author Contribution and Conflict of Interest Declaration Information

All authors contributed equally to the article. There is no conflict of interest.

References

Abrams, M., Hook, S. & Ramachandran, B. (2008). Advanced Spaceborne Thermal Emission and Reflection Radiometer (ASTER) User Handbook, Version 2.

Aghababaei, M., Ebrahimi, A., Naghipour, A.A., Asadi, E., Perez-Suay, A. & Morata, M. (2022). Introducing ARTMO's machine-learning classification algorithms toolbox: application to plant-type detection in a semi-steppe Iranian landscape, *Remote Sens-Basel*, 14, 4452.

Akın, T. & Gül, A. (2020). Isparta-Atabey yöresinin ekoturizm potansiyeli ve turizm rotalarının belirlenmesi. *Journal of Architectural Sciences and Applications*, 5(2), 221-240. https://doi.org/10.30785/mbud.793234

Asam, S., Gessner, U., Gonzalez, R.A., Wenzl, M., Kriese, J. & Kuenzer, C. (2022). Mapping crop types of Germany by combining temporal statistical metrics of Sentinel-1 and Sentinel-2 time series with LPIS data, *Remote Sens-Basel*, 14(13), 2981, 2022.

Barazzetti, L., Gianinetto, M. & Scaioni, M. (2016). Radiometric Normalization with Multi-image Pseudo-invariant Features, Fourth International Conference on Remote Sensing and Geoinformation of the Environment (Rscy2016), Paphos, Cyprus, Vol. 9688, 4-8 April 2016.

Biday, S. G. & Bhosle, U. (2012). Relative radiometric correction of multitemporal Satellite Imagery using fourier and wavelet transform, *J. Indian Soc Remote*, 40, 201-13.

Boussadia-Omari, L., Ouillon, S., Hirche A., Salamani, M., Guettouche, M. S. & Ihaddaden, A. (2021). Contribution of phytoecological data to spatialize soil erosion: Application of the RUSLE model in the Algerian atlas, *Int Soil Water Conse*., 9, 502-19.

Bujan, S., Guerra-Hernandez, J., Gonzalez-Ferreiro, E. & Miranda, D. (2021). Forest road detection using LiDAR data and hybrid classification, *Remote Sens-Basel*, 13(3), 393.

Chavez, P. S. (1988). An improved dark-object subtraction technique for atmospheric scattering correction of multispectral data, *Remote Sens Environ*., 24, 459-79.

Chavez, P. S. (1996). Image-based atmospheric corrections revisited and improved, *Photogramm Eng Rem S.,* 62, 1025-36.

Chetia, S., Saikia, A., Basumatary, M. & Sahariah, D. (2020). When the heat is on: Urbanization and land surface temperature in Guwahati, India, *Acta Geophys*, 68, 891-901, 2020.

Du, Y., Teillet, P. M. & Cihlar, J. (2002). Radiometric normalization of multitemporal high-resolution satellite images with quality control for land cover change detection, *Remote Sensing of Environment,* 82(1), 123-134, ISSN 0034-4257. doi.org/10.1016/S0034-4257(02)00029-9.

El Hajj, M., Begue, A., Lafrance, B., Hagolle, O., Dedieu, G. & Rumeau, M. (2008). Relative radiometric normalization and atmospheric correction of a SPOT 5 time series, *Sensors-Basel*, 8, 2774-91.

El Mortaji, N., Wahbi, M., Kazzi, M.A., Alaoui, O.Y., Boulaassal, H. & Maatouk, M. (2022). High resolution land cover mapping and crop classification in the Loukkos watershed (Northern Morocco): An approach using SAR Sentinel-1 time series, *Rev Teledetec*., 60, 47-69, 2022.

Garcia-Pardo, K. A., Moreno-Rangel, D., Dominguez-Amarillo, S. & Garcia-Chavez, J. R. (2022). Remote sensing for the assessment of ecosystem services provided by urban A review of the methods, *Urban for Urban Gree*., 74, 127636, 2022.

Gasparovic, M. & Dobrinic, D. (2021). Green ınfrastructure mapping in urban areas using sentinel-1 imagery, *Croat J. for Eng.,* 42, 336-55, 2021.

Getachew, B. & Manjunatha, B. R. (2022). Impacts of land-use change on the hydrology of Lake Tana Basin, Upper Blue Nile River Basin, Ethiopia, *Glob Chall*., 6, 2200041, 2022.

Ghaseminik, F., Aghamohammadi, H. & Azadbakht, M. (2021). Land cover mapping of urban environments using multispectral LiDAR data under data imbalance, *Remote Sens Appl.,* 100449, 21, 2021

Gu, Z. J., Shi, X. Z., Li, L., Yu, D. S., Liu, L. S. & Zhang, W. T. (2011). Using multiple radiometric correction images to estimate leaf area index, *In.t J. Remote Sens*., 32, 9441-54.

Islam, M. M., Borgqvist, H. & Kumar, L. (2019). Monitoring mangrove forest land cover changes in the coastline of Bangladesh from 1976 to 2015. *Geocarto Int*., 34, 1458-76, 2019.

İşler, B. & Aslan, Z. (2021). Bitki örtüsü ve mekânsal ve zamansal varyasyonların modellenmesi, *Journal of the Faculty of Engineering and Architecture of Gazi University,* 36, 1863-74, 2021.

Janzen, D. T., Fredeen, A.L. & Wheate, R.D. (2006). Radiometric correction techniques and accuracy assessment for Landsat TM data in remote forested regions, *Can. J. Remote Sens*., 32, 330-40.

Jenerowicz, A., Kaczynski, R., Siok, K. & Palkiewicz, K. (2019). Change detection of urban area based on multi-sensor imagery, *Remote Sensing Technologies and Applications in Urban Environments* IV, 11157, 126-132.

Karaca, A. C. & Güllü, M. K. (2019). Menderes ilçesindeki orman yangınının süperpiksel bölütleme temelli arama yöntemiyle tespiti, *Journal of the Faculty of Engineering and Architecture of Gazi University*, 34, 1061-76.

Khatami, R., Southworth, J., Muir, C., Caughlin, T., Ayana, A. N. & Brown, D. G. (2020). Operational large-area land-cover mapping: An Ethiopia case study. *Remote Sens.-Basel*, 12, 954.

Khorrami, B., Gunduz, O., Patel, N., Ghouzlane, S. & Najar, M. (2019). Land surface temperature anomalies in response to changes in forest cover, *Int. J. Eng. Geosci*., 4, 149-56, 2019.

Kiage, L. M., Liu, K. B., Walker, N. D., Lam, N. & Huh, O. K. (2007). Recent land-cover/use change associated with land degradation in the Lake Baringo catchment, Kenya, East Africa: evidence from Landsat TM and ETM, *Int. J. Remote Sens*., 28, 4285-309.

Lelong, C. & Herimandimby, H. (2022). Land use / land cover map of Vavatenina region (Madagascar) produced by object-based analysis of very high spatial resolution satellite images and geospatial reference data, *Data Brief*, 44, 108517, 2022.

Liu, S. H., Lin, C. W., Chen, Y. R. & Tseng, C. M. (2012). Automatic radiometric normalization with genetic algorithms and a Kriging model, *Comput Geosci-Uk*, 43, 42-51.

Liu, Y. K., Long, T. F., Jiao, W. L., He, G. J., Chen, B. & Huang, P. (2022). A General Relative Radiometric Correction Method for Vignetting and Chromatic Aberration of Multiple CCDs: Take the Chinese Series of Gaofen Satellite Level-0 Images for Example, *Ieee T Geosci Remote*, 60, 1-25.

Lobo, F. L., Costa, M. P. F. & Novo, E. M. L. M. (2015). Time-series analysis of Landsat-MSS/TM/OLI images over Amazonian waters impacted by gold mining activities, *Remote Sens Environ*., 157, 170-84.

Lopez-Serrano, P. M., Corral-Rivas, J. J., Diaz-Varela, R. A. & Alvarez-Gonzalez, J. G., Lopez-Sanchez C. A. (2016). Evaluation of Radiometric and Atmospheric Correction Algorithms for Aboveground Forest Biomass Estimation Using Landsat 5 TM Data, *Remote Sens-Basel*, 8(5), 369.

Luo, X., Tong, X. H., Hu, Z. W. & Wu, G. F. (2020). Improving Urban land cover/use mapping by ıntegrating a hybrid convolutional neural network and an automatic training sample expanding strategy, *Remote Sens-Basel,* 12(14), 2292, 2020.

MGM (2022). Meteoroloji Genel Müdürlüğü https://www.mgm.gov.tr/veridegerlendirme/il-ve-ilceler-istatistik.aspx?k=A&m=MERSIN Erişim: 27.07.2022

Prieto-Amparan, J. A., Villarreal-Guerrero, F., Martinez-Salvador, M., Manjarrez-Dominguez, C., Santellano-Estrada, E. & Pinedo-Alvarez, A. (2018). Atmospheric and radiometric correction algorithms for the multitemporal assessment of Grasslands productivity, *Remote Sens-Basel*, 10(2), 219.

Pudale, S. R. & Bhosle, U. V. (2007). Comparative study of relative radiometric normalization techniques for Resourcesat1 LISS III sensor images, Iccima: International Conference on Computational Intelligence and Multimedia Applications, Sivakasi, Tamil Nadu, India, Vol III, 233-239, 13-15.

Purwanto, A. D., Wikantika, K., Deliar, A. & Darmawan, S. (2023). Decision tree and random forest classification algorithms for mangrove forest mapping in Sembilang National Park, Indonesia, *Remote Sens-Basel*, 15(1), 16, 2023.

Rahman, M. M., Hay, G.J., Couloigner, I., Hemachandran, B. & Bailin, J. (2015). A comparison of four relative radiometric normalization (RRN) techniques for mosaicing H-res multi-temporal thermal infrared (TIR) flight-lines of a complex urban scene, *Isprs J Photogramm*., 106, 82-94.

Rauf, U., Qureshi, W. S., Jabbar, H., Zeb, A., Mirza, A. & Alanazi, E. (2022). A new method for pixel classification for rice variety identification using spectral and time series data from Sentinel-2 satellite imagery, *Comput Electron Agr.,* 193, 106731.

Rostami, N. & Fathizad, H. (2022). Spatial and temporal changes of land uses and its relationship with surface temperature in western Iran, *Atmosfera,* 35, 701-17, 2022.

Ruiz, L. F. C., Dematte, J. A. M., Safanelli, J. L., Rizzo, R., Silvero, N. E. Q. & Rosin, N. A. (2022). Obtaining high-resolution synthetic soil imagery for topsoil mapping, *Remote Sens Lett*., 13, 107-14, 2022.

Sadeghi, V., Ahmadi, F. F. & Ebadi, H. (2017). A new automatic regression-based approach for relative radiometric normalization of multitemporal satellite imagery, *Comput Appl Math*., 36, 825-42.

Scheidt, S., Ramsey, M. & Lancaster, N. (2008). Radiometric normalization and image mosaic generation of ASTER thermal infrared data: An application to extensive sand sheets and dune fields, *Remote Sensing of Environment*, 112(3), 920-933, ISSN 0034-4257. doi.org/10.1016/j.rse.2007.06.020.

Schroeder, T. A., Cohen, W. B., Song, C. H., Canty, M. J. & Yang, Z. Q. (2006). Radiometric correction of multi-temporal Landsat data for characterization of early successional forest patterns in western Oregon, *Remote Sens Environ.,* 103, 16-26.

Schott, J. R., Salvaggio, C. & Volchok, W. J. (1988). Radiometric Scene Normalization Using Pseudoinvariant Features, *Remote Sens Environ*., 26 (1), 1-14.

Tan, K. C., Lim, H. S., MatJafri, M. Z. & Abdullah, K. (2012). A comparison of radiometric correction techniques in the evaluation of the relationship between LST and NDVI in Landsat imagery, *Environ Monit Assess*., 184, 3813-29.

Tassri, N., Danoedoro, P. & Widayani, P. (2019). Multitemporal analysis of vegetated land cover changes related to tin mining activity in bangka regency using landsat ımagery, Sixth Geoinformation Science Symposium, Yokyakarta, Indonesia, *SPIE* 11311, 1131104, 26-27 August 2019.

Tavares, P. A., Beltrao, N. E. S., Guimaraes, U. S. & Teodoro, A. C. (2019). Integration of Sentinel-1 and Sentinel-2 for classification and LULC mapping in the urban area of Belem, Eastern Brazilian Amazon, Sensors-Basel, 19(5), 1140, 2019.

Ul, Din, S. & Mak, H. W. L. (2021). Retrieval of land-use/land cover change (lucc) maps and urban expansion dynamics of hyderabad, pakistan via landsat datasets and support vector machine framework, Remote Sens-Basel., 13(16), 3337, 2021.

Yang, X. J. & Lo, C. P. (2000) Relative radiometric normalization performance for change detection from multi-date satellite images, *Photogramm Eng Rem S*., 66, 967-80.

Yuan, D. & Elvidge, C. D. (1996). Comparison of relative radiometric normalization techniques, *Isprs J Photogramm.,* 51, 117-26.